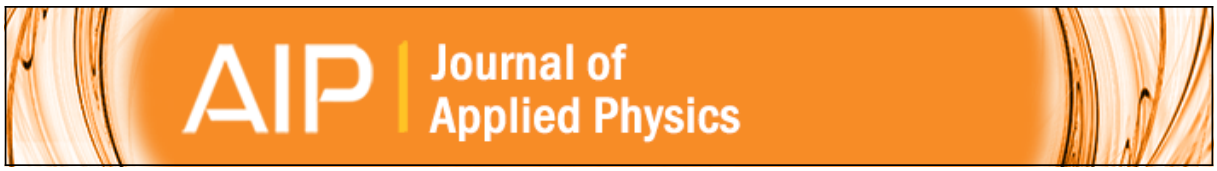

Structural and optical properties of Al-Tb/SiO2 multilayers fabricated by electron beam evaporation

O. Blázquez, J. López-Vidrier, L. López-Conesa, M. Busquets-Masó, S. Estradé, F. Peiró, S. Hernández, and B. Garrido

Citation: Journal of Applied Physics **120**, 135302 (2016); doi: 10.1063/1.4964110

View online: http://dx.doi.org/10.1063/1.4964110

View Table of Contents: http://scitation.aip.org/content/aip/journal/jap/120/13?ver=pdfcov

Published by the AIP Publishing

Structural and optical properties of Al-Tb/SiO_2 multilayers fabricated by electron beam evaporation

O. Blázquez,[a] J. López-Vidrier,[b] L. López-Conesa, M. Busquets-Masó, S. Estradé, F. Peiró, S. Hernández, and B. Garrido
MIND–IN²UB, Department of Engineering: Electronics, Universitat de Barcelona, Martí i Franquès 1, E-08028 Barcelona, Spain

(Received 28 June 2016; accepted 20 September 2016; published online 4 October 2016)

Light emitting Al-Tb/SiO_2 nanomultilayers (NMLs) for optoelectronic applications have been produced and characterized. The active layers were deposited by electron beam evaporation onto crystalline silicon substrates, by alternatively evaporating nanometric layers of Al, Tb, and SiO_2. After deposition, all samples were submitted to an annealing treatment for 1 h in N_2 atmosphere at different temperatures, ranging from 700 to 1100 °C. Transmission electron microscopy confirmed the NML structure quality, and by complementing the measurements with electron energy-loss spectroscopy, the chemical composition of the multilayers was determined at the nanoscopic level. The average composition was also measured by X-ray photoelectron spectroscopy (XPS), revealing that samples containing Al are highly oxidized. Photoluminescence experiments exhibit narrow emission lines ascribed to Tb^{3+} ions in all samples (both as-deposited and annealed ones), together with a broadband related to SiO_2 defects. The Tb-related emission intensity in the sample annealed at 1100 °C is more than one order of magnitude higher than identical samples without Al. These effects have been ascribed to the higher matrix quality, less SiO_2 defects emitting, and a better Tb^{3+} configuration in the SiO_2 matrix thanks to the higher oxygen content favored by the incorporation of Al atoms, as revealed by XPS experiments. *Published by AIP Publishing.*
[http://dx.doi.org/10.1063/1.4964110]

I. INTRODUCTION

The production of efficient light emitting devices based on silicon is of primary interest for the optoelectronic industry, especially for application in optical sensors, panel, displays, and even for indicators and illumination.[1–4] In order to achieve this goal, novel strategies have been employed. Such is the case of the semiconductor materials doped with rare earth (RE) ions, which have been widely studied due to the narrow and intense luminescence they yield, aiming at a wealth of applications.[5–8] Recently, excellent electro-optical properties have been reported on III–V semiconductors as host matrix for different RE ions, allowing for a suitable performance as light-emitting devices.[5,9] In addition, REs have been employed to develop light-emitting silicon-based materials for optoelectronic applications.[10,11] With this aim, several works have reported on RE-doped oxides such as SiO_2, Si-rich silicon oxide,[12–14] or Si-rich silicon oxynitride[15] matrices as potential candidates to become active layers in light-emitting devices. The interest in determining the optical and electronic properties of the different RE species lies in the particular electronic structure they present, which allows engineering the desired emission spectra of the active layer. Among the different RE elements, erbium is one of the most studied elements, given that its Er^{3+} oxidation state presents a characteristic emission at 1.55 μm, which is suitable for telecom applications.[16] As well, terbium and europium are interesting for their emission in the visible range, being green and red emissions typically reported for, respectively, Tb^{3+} and Eu^{3+} ions.[17] Nevertheless, clustering of RE induces the ions to become optically inactive, which notably drops their emission efficiency. In the literature, and in combination with SiO_2, aluminum has been widely employed for dispersing RE ions and thus allows for a higher RE incorporation without clustering.[18,19]

Different methods have been employed to combine these materials, being ion implantation,[16] thermal evaporation in effusion cells,[20] or plasma-enhanced chemical-vapor deposition[21] the most used ones. In a previous publication, some of the current authors reported the fabrication of Tb doped SiO_2 by means of chemical vapor deposition.[22] Other techniques such as sol-gel have shown a good optical performance,[23,24] but the difficulties for a controlled deposition and the incompatibility with planar technology constitute important drawbacks for the integration of RE in electronic and photonic devices.[25] In this work, we focus on electron beam evaporation (EBE), a physical deposition method widely employed to metalize devices, but also to grow layers from a wide range of materials, which include semiconductors. The possibility to directly evaporate pure elements and simple compounds without the need of complex chemical reactions allows also for achieving controlled deposition of thin films and reduces (or even eliminates) their contamination. The most widely used method based on EBE to combine different materials within a single thin film is by using targets with mixed compounds and under a

[a]Author to whom correspondence should be addressed. Electronic mail: oblazquez@el.ub.edu. Tel.: (+34) 93 4039176.
[b]Now at IMTEK, Faculty of Engineering, Albert-Ludwigs-University Freiburg, Georges-Köhler-Allee 103, D-79110 Freiburg, Germany.

particular atmosphere. However, the electrical current needed to properly evaporate the compounds can differ substantially and, therefore, their respective evaporation rates are difficult to control. Despite this drawback, another way to control the overall amount of the different elements takes advantage of the sequential evaporation of different materials from different targets, thus depositing consecutive nanometric layers of each of them (i.e., using the so-called nanomultilayer (NML) approach), instead of trying to do it during one single evaporation process. Therefore, this approach can be used to combine RE layers of a few nanometers with a matrix material, hence allowing for a controlled inter-ion distance in the growth direction. Finally, a post-deposition thermal treatment is then required to induce the optical activation of the ionic species, and thus making the films luminescent.

In this work, we describe the fabrication and present the structural and optical characterization of Al-Tb/SiO_2 nanomultilayered thin films. To obtain this structure, Al, Tb, and SiO_2 nanomultilayers (NMLs) were deposited using the EBE technique on a Si substrate. Different electron microscopy and high-energy spectroscopic techniques were used to characterize the multilayer structure at the nanoscale, from which the spatial distribution and binding structure of the different involved species were obtained. The overall composition of the NML structure has been determined by X-ray photoelectron spectroscopy (XPS) measurements, which also allowed gathering information about the Al effect on the Tb environment. The influence of the annealing temperature and the presence of Al atoms on the emission properties of Tb^{3+} ions were studied by means of photoluminescence (PL). Finally, the study of the PL emission lifetime of the different samples is discussed in terms of the Tb^{3+} ions atomic environment, as corroborated by structural techniques. Overall, the study highlights the possibility of employing the EBE technique, using the multilayer approach, to deposit optically active rare earth-based thin films that can lead to several optoelectronic applications.

II. EXPERIMENTAL DETAILS

Thin films of Al-Tb/SiO_2 nanomultilayers were fabricated by means of EBE technique onto crystalline (100)-Si substrate, using a PFEIFFER VACUUM Classic 500 instrument with a Ferrotec GENIUS electron beam controller and a Ferrotec CARRERA high-voltage power supply. Before deposition, substrates were cleaned with acetone, isopropyl alcohol, ethanol, and de-ionized water, and agitated ultrasonically during each process. Nanometric layers of SiO_2, Tb, and Al were alternatively deposited. In this case, the NML consists of 15 periods of Al/Tb/Al/SiO_2 layers with nominal thicknesses of 0.8, 0.4, 0.8, and 3 nm, respectively, being this configuration optimum for the optical activation of Tb^{3+} ions, as experimentally observed in a previous study.[26] In order to protect the stack from the following thermal annealing, two 10-nm SiO_2 layers were deposited at the bottom and on top of the NML structure. To elucidate the role of Al, an identical set of samples was also deposited with no Al in the NML structure (Tb/SiO_2), keeping constant the thickness of the Tb and SiO_2 layers (nominally, 0.4 and 3 nm, respectively). In Fig. 1, the cross-section schemes corresponding to both described structures are drawn.

Before the evaporation process, the base pressure in the chamber was 1.6×10^{-6} mbar and the temperature of the substrate was kept at 100 °C. The nominal deposition rates were 0.2, 0.2, and 1.0 Å/s for Al, Tb, and SiO_2, respectively, using an electron beam acceleration voltage of either 10 kV for Al or 6 kV for Tb and SiO_2. Once the deposition process was completed, the layers were submitted to an annealing treatment at temperatures of $T_{ann} = 700$, 900, or 1100 °C in a N_2 atmosphere for 1 h in a conventional tubular furnace.

A structural characterization of the cross-section NML structure was carried out on the as-deposited Al-Tb/SiO_2 sample by means of transmission electron microscopy (TEM). The sample was prepared for TEM observation by conventional mechanical polishing methods up to electron transparency. Data were acquired using a JEOL 2010 F microscope, equipped with a Schottky field emission gun and coupled to a Gatan imaging filter with 0.8 eV energy resolution. Chemical information was obtained from spatially localized electron energy-loss (EEL) spectra acquired along three periods of the NML (spectrum imaging). These spectra were co-acquired with a high angular annular dark field (HAADF) image in scanning mode (scanning-TEM, STEM), which presents a contrast corresponding to different atomic numbers. The energy-loss range was selected to be from 1000 to 2000 eV, thus covering the core-loss edges for the three elements of interest (Tb M4 and M5 edges, Al K edge, and Si K edge). No information regarding the location of oxygen could be attained due to the limitation in the energy loss of the employed energy window (O K-edge is placed around 532 keV). Areal density maps for these edges were obtained as an elemental distribution map of the multilayer. XPS measurements were also carried out using a PHI 5500 Multitechnique System, to study the overall composition and obtain information regarding the Al influence on the Tb-related binding formation, in the annealed samples at the highest temperature, with and without Al.

The optical emission properties of the NMLs were studied by means of PL spectra, exciting the samples with the

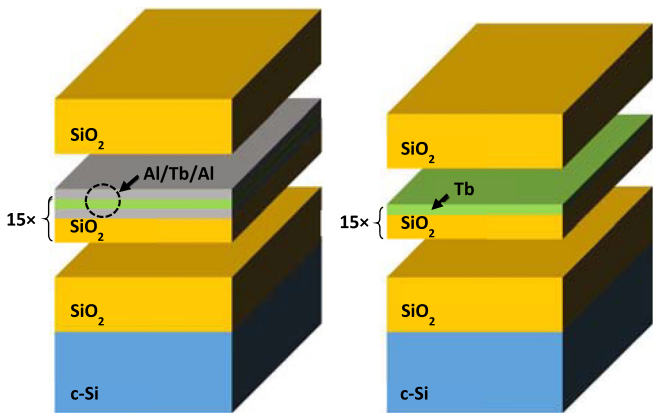

FIG. 1. Sketch of the multilayer structures employed in the present work, corresponding to 15 periods of (left) Al/Tb/Al/SiO_2 and (right) Tb/SiO_2 layers, plus the 10-nm SiO_2 protecting layers at the bottom and on top of the NML.

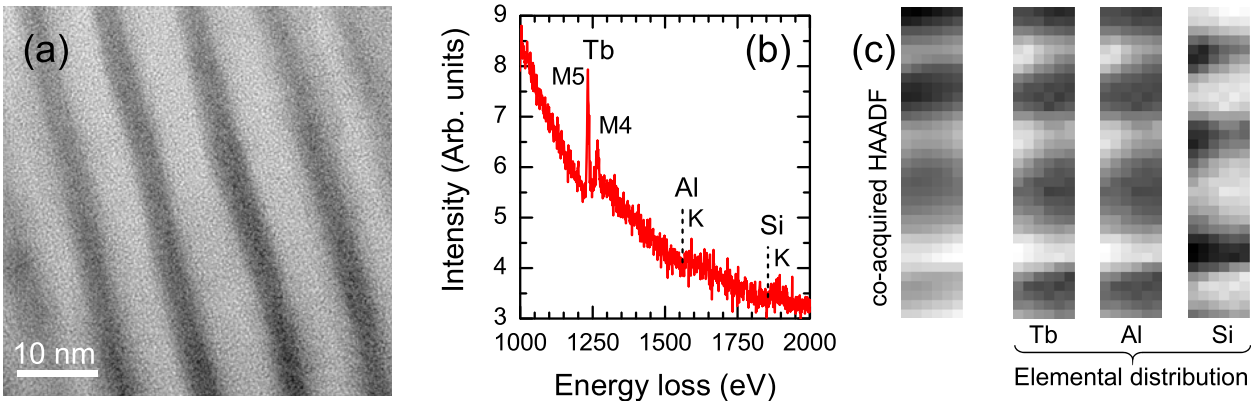

FIG. 2. (a) HRTEM image of the as-deposited Al-Tb/SiO_2 sample. (b) EEL spectrum of an area along three periods of the multilayer. (c) Co-acquired HAADF image of the same area and elemental distribution maps corresponding to each element of interest (Tb, Al, and Si) obtained from the spatially-resolved spectra.

325-nm line of a He-Cd laser. The resulting emission was collected in the visible range from 400 to 700 nm using a GaAs photomultiplier tube (PMT) coupled to a monochromator in a lock-in configuration. In order to study the Tb^{3+} radiative lifetime, the laser excitation beam was mechanically square-pulsed with a period of 20 ms and 50% duty cycle (resulting in a rise/fall time of $\sim$300 μs). The obtained PL signal from the PMT was analyzed by a digital oscilloscope.

III. RESULTS AND DISCUSSION

A. Structural characterization

To inspect the correct deposition and fabrication of the NML samples under study, their structure and composition were determined by high resolution TEM (HRTEM) and STEM-electron energy-loss spectroscopy (EELS) imaging, respectively. The HRTEM image from the as-deposited Al-Tb/SiO_2 sample exhibits an atomically-sharp interface of the Si substrate with the deposited layer. Moreover, no crystalline domains are observed in any of the regions, which implies that all layers are amorphous. In Fig. 2(a), a HRTEM image is presented, which shows the correct deposition of a nanomultilayer structure (different contrast corresponding to different material phases), with a small degree of waviness.

The as-deposited sample was further analyzed by means of HAADF and EELS spectrum imaging, in order to investigate the chemical composition of the NML stack. In Fig. 2(b), an EEL spectrum for the sample under study along three periods is presented. The spectrum clearly exhibits core-loss edges of the three interesting elements (Tb M4 and M5 edges, Al K edge, and Si K edge). An HAADF image of the same region was also taken, showing a clear difference in contrast between adjacent layers. Since HAADF contrast is sensitive to the atomic mass of the involved species, this result reveals that different atomic species are preferentially located within the NML stack, thus indicating their presence in the NML structure. Actually, the brightest contrast, corresponding to the heaviest atoms, is consistent with the spatial localization of the Tb ions within the stack. The distribution of the other present species, however, cannot be deduced from the HAADF analysis; for this reason, an EEL spectrum was co-acquired at each pixel in scanning mode. By mapping the energy-loss intensity corresponding to each element (after background subtraction), elemental distribution maps of the different species were built from the spectrum image. Fig. 2(c) shows the co-acquired HAADF image and the elemental distribution map of the three elements of interest (Tb, Al, and Si). It is clearly observed that the Si signal is spatially isolated from the Tb and Al signals. This means that Si is only located in the nominal SiO_2 layers, whereas Tb and Al signals were found to come from the same region, homogeneously distributed in an Al/Tb/Al stack and with no evidence of the nominal sandwiched structure, which implies a certain degree of intermixing of this stack and, thus, minimizing the possible Tb clustering. The overall result from the structural characterization is the presence of two distinct regions within our samples: one composed only by SiO_2 and the other one containing a mixture of Tb and Al. The

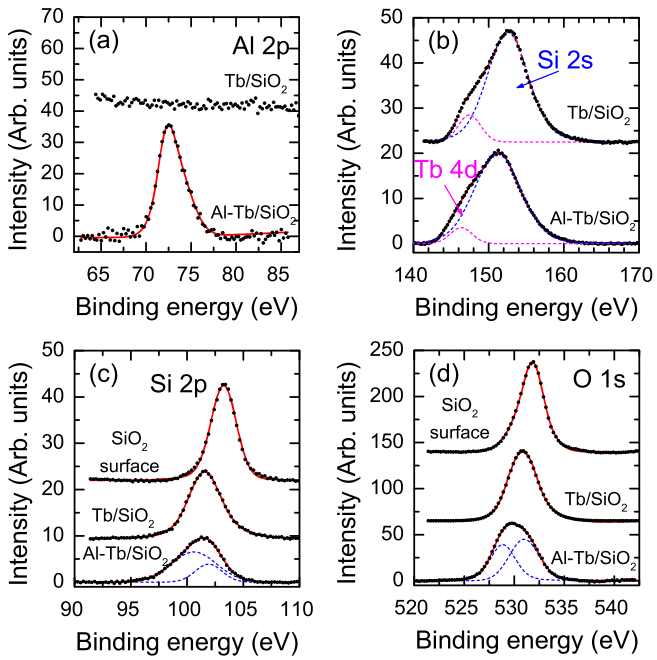

FIG. 3. XPS spectra corresponding to the NML samples with and without Al, acquired around the binding energies corresponding to Al 2p, Tb 4d, Si 2s, Si 2p, and O 1s bonds. (a) and (b) compare the presence of Al and Tb in both samples, whereas (c) and (d) focus on the stoichiometry of the present SiO_2 on the capping layer (on top of the NMLs) and within the NML stack.

measured thicknesses from both regions, as obtained from the HRTEM images [see Fig. 2(a)], are 5 and 3 nm, respectively for the SiO_2 and the Al-Tb layers, both thicker than the nominal values (3 and 2 nm, respectively).

In order to accurately determine the composition of the Al-Tb/SiO_2 structure and obtain information regarding the Al effect on the binding formation around Tb ions, XPS measurements at different depths were carried out on samples with and without Al and annealed at 1100 °C, by sputtering the layer with Ar^+ ions. As the depth resolution is around 5–10 nm, an average value of the total composition of the NMLs can be obtained. Fig. 3 exhibits the photoemission spectra obtained from the different elements within the multilayers: Si, O, Tb, and Al. In addition, Figs. 3(c) and 3(d) also present the photoemission spectra of O and Si from the top SiO_2 capping layer (the composition and stoichiometry of this SiO_2 layer could therefore be analyzed without being influenced by the rest of the nanometric layers).

The photoemission spectra corresponding to energies around the bound energy of Al 2p are displayed in Fig. 3(a). A flat spectrum (i.e., no signal) is obtained from the Tb/SiO_2 NMLs, whereas a clear contribution from Al is observed in the spectrum from the Al-Tb/SiO_2 NMLs, evidencing that Al is present only in the latter. Looking at the energy around the Tb 4d bonds, between 140 and 165 eV [see Fig. 3(b)], there is a broadband that can be deconvolved into two different contributions: one from Tb 4d (≈147 eV) and another from Si 2s bonds (≈152 eV). Their relative intensity is almost constant in the two samples, although there are small changes in their mean energy, probably associated with the influence of Al to the NML structure, which specially affect the Tb bonds. The energy window around Si 2p bonds (between 95 and 105 eV) displays one peak at ≈102 eV [see Fig. 3(c)], which broadens under the presence of Tb and Al-Tb.

The most interesting analysis, however, corresponds to binding energies near 530 eV, related to O 1s bonds [see Fig. 3(d)]. Indeed, Fig. 3 displays the photoemission spectra of the samples under study (Al-Tb/SiO_2 and Tb/SiO_2 samples) around the mentioned binding energies well within the NML structure (where Tb and Al ions are present), together with the spectrum obtained at the first surface (which corresponds to the SiO_2 capping layer, equivalent in both samples). On one hand, the O 1s peak at the surface oxide is narrow and very well defined, peaking at around 532 eV. On the other hand, the O 1s peak from the NMLs is clearly shifted to lower energies and broadened, as the presence of Tb ions influences the oxygen binding energy. Although we do not rule out the possibility of having Tb-O bonds, which are non-dominant and probably located only at the SiO_2-Tb interface, the Si-O binding energy is definitely affected by the neighboring layers. Furthermore, the effect of Al can also be highlighted within the NML, which induces a more pronounced shift to lower energies and a larger broadening of the O 1s peak. In fact, this larger broadening can be ascribed to another contribution [see the deconvolution of the bottom spectrum in Fig. 3(d)], which could be related to Al-O, Tb-O, or a combination of both bonds (in agreement with EEL results that point to an intermixing of Al and Tb at the nanoscale).

Considering the cross-section ratio from each atomic element, we have evaluated the average composition of the layers from the relative areas. The deconvolution of the binding energy contributions was performed by fitting each of them to one or two pseudo-Voigt functions. In Table I, we present the values obtained for the two samples (with and without Al), together with the values from the top SiO_2 capping layer as a reference. It is interesting to notice that the SiO_2 on the surface (identical for both samples) is stoichiometric, within the uncertainty of our measurements (below 1%). The situation for the silicon oxide within the NMLs in the sample with Al is much different: the oxygen to silicon ratio is 2.7 (see Table I), which implies an oxygen excess of 23%. Due to the fact that the same process was employed for depositing SiO_2 both on the surface and within the multilayers, a stoichiometric composition of the layers is expected there also. Therefore, the layers containing Al and Tb might have captured this extra oxygen, in agreement with the observation of Al-O or Tb-O bonds in the photoemission spectra around the O 1s binding energy. Since aluminum is easily oxidized,[27] the most probable situation is having all the Al atoms in the form of alumina (Al_2O_3). In that case, and considering that the rest of the oxygen atoms are bound to Tb ones, we estimate that there will be a minimum of 45% of Tb atoms in the form of Tb_2O_3. Even though the possibility of having Al-Tb-O ternary compounds cannot be ruled out[18,19] because Al and Tb atoms are homogeneously distributed in the Al/Tb/Al stack (as observed by TEM measurements). For the sample with no Al, the situation is much different: the oxygen-to-silicon ratio is exactly 2.0, indicating that no extra oxygen is added to the Tb layers. Actually, Tb atoms are much less chemically reactive than aluminum, which makes their oxidation difficult, taking into account the low pressure employed during deposition. Thus, in this sample, only the Tb atoms at the interface might be bound to

TABLE I. XPS peak positions, integrated areas under the curves, and evaluated atomic compositions of the top SiO_2 layer, and the Tb/SiO_2 and Al-Tb/SiO_2 NMLs.

	SiO_2		Tb/SiO_2			Al-Tb/SiO_2			
	Si 2p	O 1s	Si 2p	O 1s	Tb 4d	Si 2p	O 1s	Tb 4d	Al 2 p
Peak position (eV)	103.3	531.8	101.5	530.8	147.4	100.7 102.0	528.8 531.0	146.2	72.5
Integrated area (a.u.)	2.46	31.94	5.76	29.01	2.22	4.46	30.20	1.29	1.31
Atomic content (%)	33	67	33	66	2	24	65	1	10

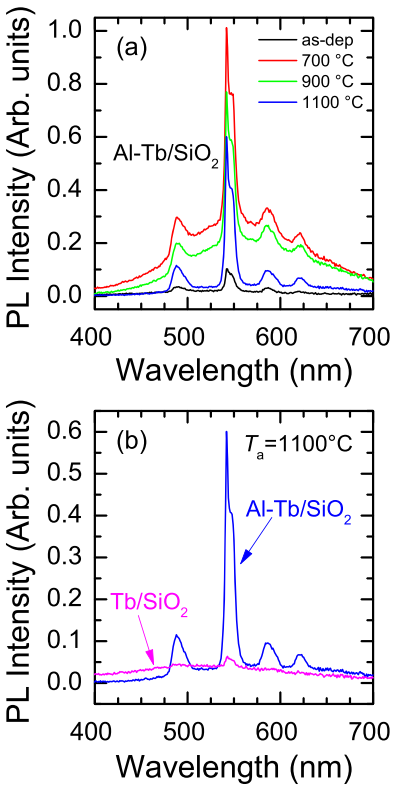

FIG. 4. (a) PL spectra corresponding to Al-Tb/SiO_2 NML samples, submitted to different annealing temperatures and excited at $\lambda_{ex} = 325$ nm. (b) Comparison of the PL spectra acquired from the NML samples with and without the presence of Al, both annealed at 1100 °C. All the spectra have been normalized to the maximum PL emission (corresponding to sample Al-Tb/SiO_2 annealed at 700 °C), thus keeping their relative intensity.

oxygen atoms from the adjacent SiO_2 layers. In conclusion, the use of Al in the Al/Tb/Al stack favors the oxidation of the Tb ions, which may have an important impact on their emission properties.

B. Optical emission of Al-Tb/SiO_2 films

The optical emission properties of the samples containing Al and submitted to different annealing temperatures were studied by means of PL by exciting the films with the $\lambda = 325$ nm line of a continuous-wave He-Cd laser [see Fig. 4(a)]. For comparison purposes, we have also analyzed the samples with no Al content [see Fig. 4(b)]. Please note that the intensity from each sample has been normalized to the one with maximum emission (the sample with Al and annealed at 700 °C). There are some identical features that can be observed in all the spectra that evolve with the annealing temperature: four narrow and weak emissions and a broadband centered around 550 nm. On one hand, the former features, i.e., the narrow emission peaks, have their origin in the electronic transitions of the discrete energy levels from the Tb^{3+} ions. In particular, the observed peak positions at 488, 542, 586, and 622 nm correspond to the $^5D_4 \rightarrow {}^7F_i$ electronic transitions with $i = 6$, 5, 4, and 3, respectively (see for instance Ref. 28). On the other hand, the additional broadband contribution is ascribed to SiO_2 defects (oxygen vacancies and/or non-bridging chemical Si-O bonds).[12,13,16] It is interesting to follow the intensity evolution of these two different contributions, as observed in Fig. 4(a): the spectra show a sudden increase of the Tb-related emission after the annealing treatment, together with the increase of the defects band emission, favoring the optical activation of both Tb^{3+} ions and matrix defects. This latter emission reaches its maximum at 700 °C and decreases again for higher T_{ann}, whereas the emission from the Tb^{3+} ions is kept almost constant for the three different annealing treatments. This evolution is linked to the nature of these two contributions to the PL spectra, and both the absorption and emission processes should be taken into account.

As we demonstrated by XPS, our SiO_2 films are stoichiometric, but most likely they do not reach the quality levels of thermal SiO_2. Therefore, we expect deep defect levels in our material, an assumption that is supported by the observed broad emission in the spectra. This emission is coming from the absorption (and thus excitation) and subsequent relaxation of defect states, and provides no emission when the amount of non-radiative paths is too large (as happens in the as-deposited sample); on the contrary, the emission enhancement at higher temperatures is due to a reduction of non-radiative defects while activating radiative ones (which, as observed by PL, requires high annealing temperatures), reaching a maximum emission at 700 °C; higher annealing temperatures improve the long-range atomic ordering of the oxide matrix (i.e., its structural arrangement),[14] consequently reducing the overall presence of defects and thus decreasing their emission. The situation is slightly different for Tb^{3+} ions emission: in this case, in order to excite optically active Tb^{3+} ions, the excitation energy must match the transition energy involving the $^5D_4$ electronic level (i.e., resonant conditions). When the exact matching by incident radiation is not possible, the latter may still be absorbed by the matrix and partially transferred to the Tb^{3+} ions (into the $^5D_4$ electronic level) with the consequent radiative decay to the ^7F_i levels that gives rise to the observed PL. As no apparent energy level is found in Tb^{3+} species (see Ref. 29), the simple observation of those narrow emissions evidences that the 325 nm excitation (~3.8 eV) accomplishes the second case, i.e., a SiO_2 matrix absorption followed by energy transfer to Tb^{3+} ions, and a consequent radiative decay. Therefore, the incoming photons on such a material structure are expected to excite the intra-band gap (defects-induced) electronic levels within the host SiO_2 matrix and transfer that energy to Tb^{3+} ions.[30] Regarding the temperature evolution of the Tb-related PL emission intensity, annealing properly rearranges the local environment of Tb, so that the REs become optically active; indeed, this is the reason why a huge emission increase is observed after annealing at 700 °C. Higher annealing temperatures do not substantially improve the O environment of Tb, and hence no further Tb-related PL intensity increase takes place, although, as already discussed, they contribute to the reduction of the emission from SiO_2 defects.

When comparing the emission of samples annealed at 1100 °C with and without Al [see Fig. 4(b)], one can observe a dramatic intensity reduction from Tb-related emission, which evidences that Al doping induces a higher optical activation of Tb^{3+} ions. Indeed, this pattern is repeated under all

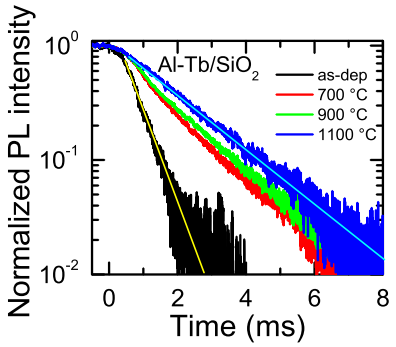

FIG. 5. Normalized time-resolved PL of Al-Tb/SiO_2 samples at 542 nm, both as-deposited and annealed at different temperatures.

other annealing conditions (not shown). Actually, XPS analysis has demonstrated that the presence of Al propitiates the NML oxidation, having an extra 23% of O atoms inside the Al-Tb layers. Thus, the inclusion of Al atoms contributes to the oxidation of the Tb atoms environment, some of them easily reaching the 3+ oxidation state while at the same time contributing to improve the stoichiometry (and the quality) of the deposited SiO_2. These facts are supported by the PL observations, which evidence that the presence of Al contributes to improve the optical activation of Tb^{3+} ions, whereas a high T_{ann} notably reduces the emission from the matrix defects (also compatible with a better SiO_2 quality).

To complement the information provided by the spectrally resolved PL measurements, the emission dynamics of the samples was also investigated by analyzing the PL emission decay, monitoring the $^5D_4 \rightarrow {}^7F_5$ transition ($\lambda = 542$ nm). For this, the He-Cd laser was mechanically square-pulsed with a period of 20 ms, allowing for a time resolution of around 0.3 ms. In Fig. 5, the PL emission decay curves of the Al-Tb/SiO_2 samples are displayed just after the laser excitation is cut, for the different annealing temperatures. Please note that the monitored wavelength presents a high contribution of defects to PL emission; however, since defects in SiO_2 typically exhibit decay times faster than 100 ns (because of high population of non-radiative centers),[31] the following analysis on the (slower-lifetime) Tb-related PL decay is not affected by this occurrence. In the case of the as-deposited sample, a single exponential function was employed to adjust the data, obtaining a good fit that revealed a decay time of $\tau_{decay} = 0.5$ ms. This value, although in good agreement with reported values in the literature on similar systems, is still too close to the time resolution of the setup, so that further conclusions are prevented in this work. After the annealing process, the measurements exhibit a different behavior consisting of two different decay times, a first fast decay (τ_f) followed by a slower one (τ_s), as can be observed for the samples with $T_{ann} = 700$ and 900 °C. A two-exponential fit was used to estimate both lifetime values, thus obtaining values slightly longer than for the as-deposited sample (and markedly longer than the setup time resolution), $\tau_f = 1.2$ ms and $\tau_s = 1.7$ ms. Finally, emission corresponding to the sample annealed at the highest temperature, $T_{ann} = 1100$ °C, exhibits only one decay time, which corresponds to the longest (τ_s) one observed in the intermediate-temperature annealed samples. It should be mentioned here that the sample without Al (not shown in the figure) presented a decay time of around 0.6 ms, similar to the as-deposited sample; this indicates that the contribution of Al to Tb^{3+} emission only takes place after the annealing treatment.

The two different decay times revealed at low annealing temperatures (700 and 900 °C), associated with the recombination lifetime within the rare earth ions, indicate that there are Tb^{3+} ions in two different optically active spatial configurations.[24,32] As the annealing temperature increases, the faster decay time becomes longer until it reaches the slower one and only one decay time is observed ($\tau_s \approx 1.7$ ms). In fact, different recombination lifetimes are ascribed to a different combination of radiative and non-radiative processes taking place within the material system (Tb ions and matrix defects); in this frame, the increase of τ_{decay} after increasing the annealing temperature can be associated with a reduction of non-radiative processes.[33] Actually, Tb^{3+} requires a C_{4V} symmetry (a TbO_6 conformation) to be optically active, as in the case of other RE ions in the same oxidation state (such as Er^{3+} or Yb^{3+}).[34–36] This occurrence, bearing in mind the multilayer structure, can take place at the interfaces between the Al/Tb mixed stack and the SiO_2 sublayers, although the possible diffusion of oxygen from the SiO_2 sublayers to the Al/Tb stack cannot be discarded; this argument also holds for the samples containing no Al. The fact that Tb^{3+} ions are very sensitive to the presence of surrounding defects constitutes a drawback for their emission. Both the high temperature annealing and the introduction of Al in the samples modify the environment of Tb^{3+} ions by eliminating defects (mainly oxygen vacancies), generating non-bridging oxygen bonds (Al-O), and reducing the Tb-Tb cross-relaxation processes,[28] similarly to the case of Eu^{3+} in Al_2O_3-SiO_2 systems,[37] consequently increasing the luminescence lifetime and thus the total emission yield from Tb^{3+} ions. This frame is also in agreement with the higher rate of active RE under the presence of Al, as suggested by the larger excitation cross-section of the Al-Tb/SiO_2 multilayers. Indeed, the latter statement can be correlated to the binding structure modification undergone by Tb-doped NML when introducing Al, as supported by the XPS analysis.

The discussion and stated hypotheses within the present work, although in reasonable agreement with the presented experimental results, should be supported by a further analysis focusing on the local environment of Tb^{3+} ions. Nevertheless, we have shown here that, by using the EBE technique to directly deposit Tb and SiO_2 multilayers, we can achieve active Tb^{3+} ions within a SiO_2 matrix, and that we can strongly enhance their emission yield by introducing Al atoms in a controlled manner within the multilayer system. As a consequence, this system can be considered for future optoelectronic applications requiring visible light emission (such as light-emitting devices) or discrete and coherent emission energies (RE-based lasing systems).

IV. CONCLUSIONS

Al-Tb/SiO_2 multilayers were fabricated by means of electron beam evaporation by alternatively evaporating

nanometric SiO_2 and sandwiching the Tb layer between two Al layers. The resulting nanostructures were submitted to different annealing temperatures. A structural characterization of the samples was carried out via TEM, which confirmed the deposited NML structure. A chemical analysis of the composition at the nanoscale by means of HAADF and EELS showed that Tb and Al thin layers are homogeneously mixed and adequately separated by the SiO_2 layers. XPS measurements were also performed on samples with and without Al, indicating that the presence of Al modifies the binding structure of O 1s orbitals, probably inducing a rearrangement of the Tb oxygen environment. The PL spectra of all samples exhibit narrow Tb^{3+} ions- and broad defects-related emission, whose relative yield varies with the temperature of the post-deposition annealing treatment and the presence of Al. A study of the PL decay time showed two different values in annealed samples containing Al, $\tau_f = 1.2$ ms and $\tau_s = 1.7$ ms, which evidences that two different atomic arrangements might exist surrounding the RE ions. The above mentioned results were discussed in terms of the environment of the REs under different conditions: the introduction of Al generates Al-O bonds when the NML is annealed, eliminating the bridging oxygen atoms and enhancing the Tb^{3+} optical activation, consequently improving the PL emission intensity of REs by more than one order of magnitude. The above discussed experimental results evidence that the combination of electron beam evaporation with a multilayer approach becomes an appropriate method for the fabrication of luminescent Al-Tb/SiO_2 NMLs, which can be applied in the field of visible-light emission optoelectronics and lasing.

ACKNOWLEDGMENTS

This work was financially supported by the Spanish Ministry of Economy and Competitiveness (Project Nos. TEC2012-38540-C02-01, CSD2009-2013, MAT-2010-16407, and MAT2013-41506). O.B. also acknowledges the subprogram "*Ayudas para Contratos Predoctorales para la Formación de Doctores*" from the Spanish Ministry of Economy and Competitiveness for economical support.

[1]O. Boyraz and B. Jalali, Opt. Express **12**, 5269–5273 (2004).
[2]G. T. Reed, G. Mashanovich, F. Y. Gardes, and D. J. Thomson, Nat. Photonics **4**, 518–526 (2010).
[3]D. J. Moss, R. Morandotti, A. L. Gaeta, and M. Lipson, Nat. Photonics **7**, 597–607 (2013).
[4]A. Rickman, Nat. Photonics **8**, 579–582 (2014).
[5]A. J. Steckl and R. Birkhahn, Appl. Phys. Lett. **73**, 1700 (1998).
[6]A. J. Steckl, M. Garter, D. S. Lee, J. Heikenfeld, and R. Birkhahn, Appl. Phys. Lett. **75**, 2184 (1999).
[7]J. Heikenfeld, M. Garter, D. S. Lee, R. Birkhahn, and A. J. Steckl, Appl. Phys. Lett. **75**, 1189 (1999).
[8]Q. Wang and A. J. Steckl, Appl. Phys. Lett. **82**, 502 (2003).
[9]*Rare-Earth Doped III-Nitrides for Optoelectronic and Spintronic Applications*, Series: Topics in Applied Physics, Vol. 124, edited by K. P. O'Donnell and W. Dierolf (Springer, Dordrecht, The Netherlands, 2010).
[10]A. J. Kenyon, Prog. Quantum Electron. **26**, 225–284 (2002).
[11]S. Yerci, R. Li, and L. Dal Negro, Appl. Phys. Lett. **97**, 081109 (2010).
[12]M. Kulakci and R. Turan, J. Lumin. **137**, 37 (2013).
[13]A. Podhorodecki, L. W. Golacki, G. Zatryb, J. Misiewicz, J. Wang, W. Jadwisienczak, K. Fedus, J. Wojcik, P. R. J. Wilson, and P. Mascher, J. Appl. Phys. **115**, 143510 (2014).
[14]A. Podhorodecki, G. Zatryb, J. Misiewicz, J. Wojcik, P. R. J. Wilson, and P. Mascher, Nanotechnology **23**, 475707 (2012).
[15]Y. Berencén, R. Wutzler, L. Rebohle, D. Hiller, J. M. Ramírez, J. A. Rodríguez, W. Skorupa, and B. Garrido, Appl. Phys. Lett. **103**, 111102 (2013).
[16]L. Rebohle and W. Skorupa, *Rare-Earth Implanted MOS Devices for Silicon Photonics*, Springer Series in Materials Science (Springer, 2010).
[17]W. Chen, R. Sammynaiken, and Y. Huang, J. Appl. Phys. **88**, 1424 (2000).
[18]G. G. Vienne, W. S. Brocklesby, R. S. Brown, Z. J. Chen, J. D. Minelly, J. E. Roman, and D. N. Payne, Opt. Fiber Technol. **2**, 387 (1996).
[19]G. Alombert-Goget, N. Gaumer, J. Obriot, A. Rammal, S. Chaussedent, A. Monteil, H. Portales, A. Chiasera, and M. Ferrari, J. Non-Cryst. Solids **351**, 1754 (2005).
[20]A. T. Fromhold, Jr. and W. D. Foster, Electrocomponent Sci. Technol. **3**, 51–62 (1976).
[21]M. Yoshihara, A. Sekiya, T. Morita, K. Ishii, S. Shimoto, S. Sakai, and Y. Ohki, J. Phys. D: Appl. Phys. **30**, 1908–1912 (1997).
[22]J. M. Ramírez, J. Wojcik, Y. Berencén, A. Ruiz-Caridad, S. Estradé, F. Peiró, P. Mascher, and B. Garrido, Nanotechnology **26**, 085203 (2015).
[23]E. M. Yeatman, M. M. Ahmad, O. McCarthy, A. Martucci, and M. Guglielmi, J. Sol-Gel Sci. Technol. **19**(1–3), 231–236 (2000).
[24]A. J. Silversmith, N. T. T. Nguyen, B. W. Sullivan, D. M. Boye, C. Ortiz, and K. R. Hoffman, J. Lumin. **128**, 931–933 (2008).
[25]J. M. Ramírez, Y. Berencén, L. López-Conesa, J. M. Rebled, F. Peiró, and B. Garrido, Appl. Phys. Lett. **103**, 081102 (2013).
[26]O. Blázquez, J. M. Ramírez, J. López-Vidrier, Y. Berencén, S. Hernández, P. Sanchis, and B. Garrido, Proc. SPIE **9520**, 95200K-1 (2015).
[27]N. Maiti, A. Biswas, R. B. Tokas, D. Bhattacharyya, S. N. Jha, U. P. Deshpande, U. D. Barve, M. S. Bhatia, and A. K. Das, Vacuum **85**, 214 (2010).
[28]F. S. Richardson, Chem. Rev. **82**, 541 (1982).
[29]J. Vuojola and T. Soukka, Methods Appl. Fluoresc. **2**, 012001 (2014).
[30]C. Armellini, M. Ferrari, M. Montagna, G. Pucker, C. Bernard, and A. Monteil, J. Non-Cryst. Solids **245**, 115–121 (1999).
[31]K. S. Min, K. V. Shcheglov, C. M. Yang, H. A. Atwater, M. L. Brongersma, and A. Polman, Appl. Phys. Lett. **69**, 2033 (1996).
[32]V. H. Romero, E. De la Rosa, T. López-Luke, P. Salas, and C. Angeles-Chavez, J. Phys. D: Appl. Phys. **43**, 465105 (2010).
[33]K. S. Seol, T. Karasawa, Y. Ohki, H. Nishikawa, and M. Takiyama, Microelectron. Eng. **36**, 193 (1997).
[34]A. J. Steckl, J. Heikenfeld, D. S. Lee, and M. Garter, Mater. Sci. Eng. B **81**, 97–101 (2001).
[35]M. Ishii, S. Komuro, T. Morikawa, and Y. Aoyagi, J. Appl. Phys. **89**, 3679 (2001).
[36]M. Lluscà, J. López-Vidrier, A. Antony, S. Hernández, B. Garrido, and J. Bertomeu, Thin Solid Films **562**, 456 (2014).
[37]M. Nogami and Y. Abe, J. Non-Cryst. Solids **197**, 73 (1996).